Title

Terrain-Shape Indices for Modeling Soil Moisture Dynamics

Journal

Soil Science Society of America Journal, 77(5)

ISSN

0361-5995

Authors

Beaudette, Dylan E
Dahlgren, Randy A
O'Geen, Anthony T

Publication Date

2013-09-01

DOI

10.2136/sssaj2013.02.0048

Peer reviewed

Published September 20, 2013

Terrain-Shape Indices for Modeling Soil Moisture Dynamics

Dylan E. Beaudette*
USDA-NRCS
19777 Greenley Rd.
Sonora, CA 95370

Randy A. Dahlgren
Anthony T. O'Geen
Department of Land, Air and Water Resources
Plant and Environmental Sciences
University of California
One Shields Ave.
Davis, CA 95616

This study examined spatial and temporal relationships between measured soil moisture and terrain-based proxies for soil moisture dynamics. Two catenas were intensively sampled reflecting a mosaic of differences in degree of soil development in California's Sierra Foothill Region. A catena containing weakly developed soils (Haploxerepts + Haploxeralfs) formed from granitic parent materials was compared to a catena of well-developed soils (Haploxeralfs and Palexeralfs) formed from metavolcanic parent materials. Soil moisture was monitored at 10-, 30-, and 50-cm depths in 15 profiles in the granitic catena and 100 profiles in the metavolcanic catena. Seven post-rainfall periods during the 2008–2009 water year were selected to compare terrain shape indices and measured soil moisture. No single terrain index (slope, tangential curvature, profile curvature, mean curvature, topographic prominence, terrain characterization index, and compound topographic index [CTI]) consistently described variability in mean water content or dry-down rates, across depth or space. However, within the granitic catena, a combination of CTI and modeled beam radiance consistently accounted for 30 to 70% of the total variance in mean water content at 10 cm, and 10 to 40% at 30- and 50-cm depths. The predictive capacity of digital elevation model (DEM)-derived terrain shape indices for soil moisture dynamics varied widely in time and space, and was influenced by spatial patterns in the degree of soil development. Efforts to describe soil moisture variability are an important attribute of digital soil mapping (DSM). Moreover, soil variability influences soil moisture dynamics, thus synergistic activities are needed to integrate landscape scale variability with digital soil mapping.

Abbreviations: CTI, compound topographic index; DEM, digital elevation model, DSM, digital soil mapping; ESRA, European Solar Radiation Atlas; ET, evapotransipiration; GPS, global positioning system; GRAD, slope gradient; MAAT, mean annual air temperature; MAP, mean annual precipitation; MCURV, mean curvature; PCURV, profile curvature; PROM, topographic prominence; PRP, post-rainfall period; RST, regularized splines in tension; RTK, real-time kinematic; SFR, Sierra Foothill Region; SFREC, Sierra Foothill Research and Extension Center; SJER, San Joaquin Experimental Range; TCI, terrain characterization index; TCURV, tangential curvature; VIF, variance inflation factor; VWC, volumetric water content; WMPD, weighted-mean particle diameter.

Landscape-scale variability in soil properties is usually driven by processes that control redistribution of sediment, precipitation, and microclimate; where the magnitude of variability is stratified by dominant soil-forming factors (Wilding et al., 1994). In many landscapes, repeating patterns of (usually overlapping) soil-forming factors give rise to predictable patterns in soil characteristics (Pennock et al., 1987). This phenomenon and its application define a paradigm for describing hydropedologic processes using field observations coupled with contextual data (aerial imagery, topographic maps, geologic maps, etc.) that are hypothesized to have a connection with active soil-forming factors (Moore et

Soil Sci. Soc. Am. J. 77:1696–1710
doi:10.2136/sssaj2013.02.0048
Received 1 Feb. 2013.
*Corresponding author (debeaudette@ucdavis.edu).

al., 1991; Hudson, 1992; Thompson et al., 2001). The accuracy of predictions based on the soil-landscape paradigm depends on careful selection and weighting of contextual information, which is usually only possible with extensive field experience and a solid understanding of pedogenic processes (Wagenet et al., 1994). The digital implementation of this approach, supported by widely available, high-resolution spatial data coupled with statistical and mapping software, has resulted in effective quantification techniques that document soil variability and also the redistribution of soil moisture over the landscape (Western et al., 1999; McBratney et al., 2003; Scull et al., 2003; Lin et al., 2006).

Most digital mapping studies focus on external "drivers" of soil formation (e.g., hillslope processes that affect the redistribution of water, sediment, and mineral weathering), with an inferred relationship to digital proxies for these drivers. Also known as soil-environmental correlation (McKenzie and Ryan, 1999) or DSM, this approach relies on fitting statistical models to soil and environmental covariates (i.e., proxies for soil-forming factors), followed by prediction at unsampled locations. At the watershed to landscape scale, slope shape, exposure, and compound metrics describing water flow or sediment accumulation are some of the major proxies used to characterize soil-forming processes (Moore et al., 1993; Thompson et al., 2001). These terrain-based metrics are calculated from DEMs (Wilson and Gallant, 2000a), making integration into soil survey investigations practical (McKenzie et al., 2000). Quantitative models based on digital proxies for hydropedologic processes, represent a promising approach for detailed (e.g., >1:24,000 scale) mapping of water dynamics in the environment (Park and van de Giesen, 2004).

Hydrologists and digital soil mappers use similar tools to describe soil- and soil moisture-variability. Topography is commonly considered one of the main static factors that affects runoff processes and the primary predictor of watershed-scale hydrology (Western et al., 1999). Slope aspect (angle), cosine-transformed aspect angle, and various models of the surface energy budget have been used as a proxy for the effects of solar radiation on soil ecohydrology (Beaudette and O'Geen, 2009). Compound topographic indices (wetness index, stream power index, potential solar radiation, etc.) have been used as proxies for hillslope-scale variability in soil moisture (Moore et al., 1991). Beven and Kirkby (1979) were among the first to incorporate the concept of the CTI into a watershed scale model (TOPMODEL) of soil moisture. Burt and Butcher (1985) found significant correlation between various terrain shape indices and depth to saturation in a 1.4-ha catchment. Western et al. (1999) published data from a comprehensive demonstration of digital proxies for soil moisture distribution at the watershed scale, based on slope, upslope contributing area, CTI, and potential solar radiation. They found that upslope contributing area was the best predictor of soil moisture in wet periods and potential solar radiation was the best predictor during dry periods. The relationships between digital proxies for soil moisture, however, are commonly site-dependent and usually poorly correlated with point measurements (Western et al., 1999; Grayson and Western, 2001; Swarowsky et al., 2011).

While terrain indices have performed well in terms of explaining variability in soil moisture in some settings, in other settings these tools have been shown to perform poorly (Western et al., 1999). Dynamic factors such as precipitation, evapotranspiration, drainage, lateral flow, and presence of water tables also govern the distribution of soil moisture in space and time (Reynolds; 1970; Takagi and Lin 2011). Moreover, soil properties such as horizon stratigraphy (e.g., claypans or duripans) and subsurface topography at the soil-bedrock interface also regulate the redistribution of soil moisture at catchment scales (Freer et al., 2002; McGlynn et al., 2002; Tromp-van Meerveld and McDonnell, 2006; Rains et al., 2006; Swarowsky et al., 2012).

In this study we evaluated commonly used digital proxies for spatial and temporal variability of soil moisture within two soil catenas containing a mosaic of soils with large differences in degree of soil development. Specific research questions included: (i) Do digital proxies describe spatial patterns in measured soil moisture that are consistent with the soil-landscape paradigm? and, (ii) Are the relationships between digital proxies and measured soil moisture consistent across differences in pedogenic development through time, and at different depths following rainfall events?

MATERIALS AND METHODS

Environmental Setting

The Sierra Foothill Region (SFR) of California spans 1.45 million ha consisting of predominately metamorphic 40% and granitic rocks 60%. Elevation ranges from 60 to 1500 m, mean annual precipitation (MAP) ranges from 200 to 1000 mm, and mean annual air temperature (MAAT) ranges from 7 to 18°C. The region has a characteristic Mediterranean climate with hot, dry summers and cool, wet winters (thermic, xeric). We studied two 30-ha landscapes representative of the landforms, ecosystems, soil types, and major lithologic bodies within the SFR (Fig. 1). The study sites have been managed for over 50 yr with low to moderate intensity cattle (*Bos taurus*) grazing.

A 30-ha collection of adjacent catenas at the San Joaquin Experimental Range (SJER), was selected to represent the rolling terrain and blue oak (*Quercus douglasii* Hook. & Arn.) savanna of granitic landscapes of the central and southern SFR. Foothill pine (*Pinus sabiniana* Douglas), buckbrush [*Ceanothus cuneatus* (Hook.) Nutt. var. *cuneatus*], and a mixture of annual grasses and forbes [(*Bromus hordeaceus* L., *B. diandrus* Roth, *Vulpia myuros* L., *B. madritensis* L., and *Erodium botrys* (Cav.) Bertol.] are found throughout the area. Tree canopy cover was estimated to be 20%, using supervised classification of panchromatic (red, green, and blue channels) from aerial imagery (SMAP algorithm (Bouman and Shapiro, 1994)). Local geology is dominated by Mesozoic granodiorite with patches of granite, tonalite, and diorite (Strand, 1967). Soils at SJER are typical of those mapped within this region: Ahwahnee (coarse-loamy, mixed, active, thermic Mollic Haploxeralfs) on summit positions, and Vista (coarse-loamy, mixed, superactive, thermic Typic Haploxerepts) on the backslope positions (Natural Resources Conservation

Service, 1990). Elevation within the SJER catena extends from 330 to 370 m, MAP is 500 mm, and MAAT is 16.0°C.

A single 30-ha headwater catchment at the Sierra Foothill Research and Extension Center (SFREC) was selected to represent the steeper and more densely wooded metamorphic landscapes of the northern SFR. Blue oak, interior live oak (*Q. wislizeni*), California black oak (*Q. kelloggii* Newb.), and foothill pine are the most common tree species in the area, with thicker stands on northern aspects. Tree canopy cover was estimated to be between 55 and 65% (Chow et al., 2009). Understory vegetation is dominated by annual grasses and forbs (*Bromus mollis* L., *Hordeum hystix* Roth, *Avena barbata* Link, *Anahallis arvensis* L., and *Geranium molle* L.) on warmer slopes, while cooler slopes are dominated by a mixture of annual grasses, forbs, and poison oak [*Toxicodendron diversilobum* (Torrey & A. Gray) E. Greene]. Local geology is dominated by Mesozoic metavolcanic rocks (greenstone) of the Smartville complex (Hacker, 1993). Dominant soils included: Sobrante (fine-loamy, mixed, active, thermic Mollic Haploxeralfs) and Timbuctoo (fine, parasesquic, thermic Typic Rhodoxeralfs), both occurring on backslope and summit positions (Natural Resources Conservation Service, 1998). Elevation within the SFREC catena extends from 160 to 410 m, MAP is 705 mm, and MAAT is 16.6°C.

Soil Sampling and Sensor Installation

Locations for soil moisture instrumentation were selected according to a *random-stratified* design (de Gruijter et al., 2006) within expert-delineated landscape positions at both catenas. Soil profiles were excavated to bedrock, morphological characteristics were described using standard soil survey techniques, and soil samples were collected by genetic horizon. A total of 15 soil profiles at SJER were instrumented with Decagon EC-5 (Decagon Devices Inc., Pullman, WA) volumetric water content (VWC) sensors at 10-, 30-, and 50-cm depths (Fig. 1). Two shallow profiles were instrumented with sensors at 10- and 30-cm depths. A total of 100 soil profiles at SFREC were instrumented with sensors, however data from only 45 of these profiles were used due to sensor failure that occurred during the 2008–2009 water year (Fig. 1). Soil moisture sensors installed in the A (10 cm), BA-Bt transition (30 cm), and middle of Bt (50 cm) horizons were used in this study. A more comprehensive description of the sensor installation is given by Swarowsky et al. (2012).

Particle-size distribution was determined by pipette method (Soil Survey Staff, 2004). Coarse fragment volume was estimated in the field. Particle-size data were associated with each soil moisture sensor according to the nearest sampled horizon. Weighted-mean particle diameter (WMPD) was computed for each horizon:

$$\mathrm{WMPD} = \frac{\sum w_i \times d_i}{\sum w_i} \qquad [1]$$

where w_i is the measured quantity (mass percent) of each size class, and d_i is the corresponding median diameter from each size class

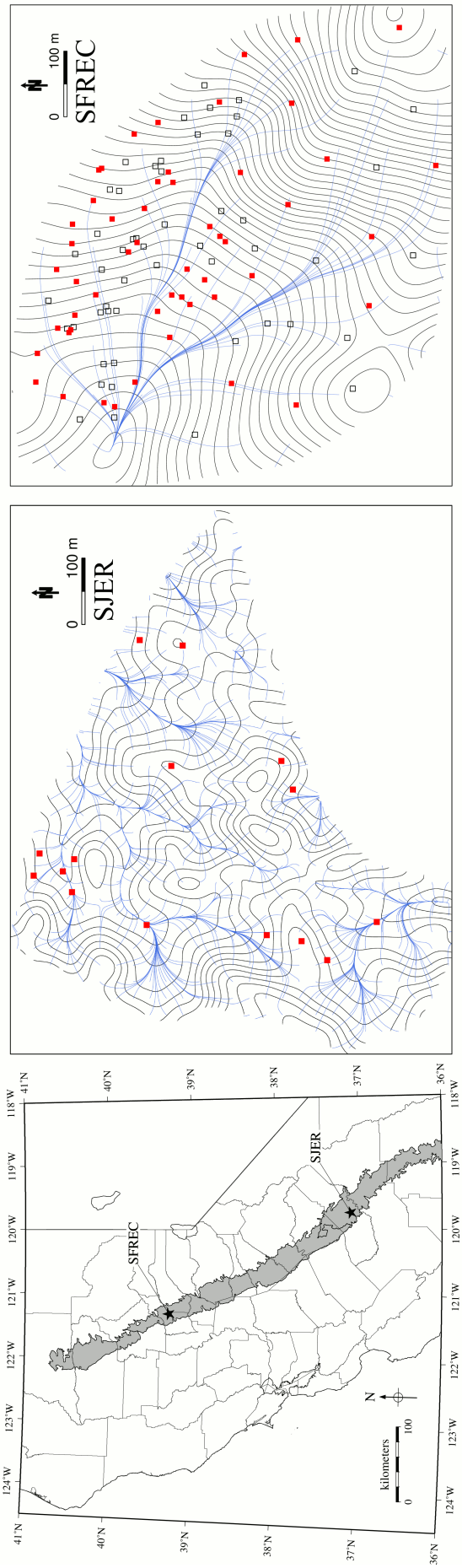

Fig. 1. Locations of the study sites (star symbols), within the Sierra Foothill Region (shaded area) of California. Instrumented locations (point symbols), elevation contours (solid black lines), and estimated paths of flow-line convergence (solid blue lines) within the San Joaquin Experimental Range (SJER) and Sierra Foothill Research and Extension Center (SFREC) study areas. Filled symbols represent locations instrumented with water content sensors. Open symbols represent locations instrumented with water content sensors that had an incomplete record of moisture data due to sensor failure.

(clay through very coarse sand). The WMPD values were used as a surrogate for water-holding capacity (Pachepsky et al., 2001).

Soil samples were used to verify the factory supplied EC-5 sensor calibration equations. Sensor failure at SJER resulted in an incomplete record of soil moisture readings between installation (November 2008) and final measurements (March 2010). However sufficient data were available for the early winter wet-up phase in November 2008 through the late spring dry-down phase in May 2009. Sensor failure was attributed primarily to burrowing rodents (pocket gophers [*Thomomys bottae*]).

Digital Terrain Modeling

A detailed elevation survey was conducted at both catenas with a Trimble R7 real-time kinematic (RTK) global positioning system (GPS) with approximately 35 observations per hectare (Trimble Navigation Limited, Sunnyvale, CA). The RTK sampling locations were determined by iteratively increasing the spacing between intersecting nodes derived from existing (USGS 10-m national elevation data) contour lines, drainage network lines, and ridge lines until root-mean-square-error of the interpolated surface stabilized. A gridded elevation model (1-m horizontal spacing) was generated via regularized splines in tension (RST) interpolation, allowing for increased smoothness of the elevation surface where GPS observations were of lower (~10 cm) vertical precision (Mitasova and Mitas, 1993).

Primary topographic parameters (slope angle, aspect angle, profile curvature [PCURV], tangential curvature [TCURV], and mean curvature [MCURV]) were generated from partial first and second derivatives of the elevation surface fit by RST interpolation (Mitasova and Hofierka, 1993). Profile curvature is interpreted as an indicator of local changes in flow velocity (Western et al., 1999). The TCURV is analogous to plan curvature (i.e., curvature along a contour line), and typically interpreted as an index of local flow convergence (Mitasova and Hofierka, 1993; Western et al., 1999). The MCURV is the mean of profile and tangential curvature, and represents areas that are predominately convex (positive values), concave (negative values), or linear (values near 0).

Secondary topographic parameters including the compound topographic index (CTI) (Wilson and Gallant, 2000b) and terrain characterization index (TCI) (Park et al., 2001) were computed within GRASS GIS (GRASS Development Team, 2009). Low CTI values correspond with regions that are (theoretically) water-shedding (2–4 in our catenas), and high CTI values correspond with regions that are water-focusing (9–11 in our catenas). The CTI values >11 to 12 correspond to locations of ephemeral streams. The TCI uses negative values to indicate local, three-dimensional focusing of water and sediment, and positive values to suggest the opposite (Park et al., 2001).

Llobera's topographic prominence index (PROM) is a relative measure of terrain ruggedness when evaluated over several scales, and a measure of relative hillslope position when evaluated at large (<1000 m^2) cartographic scales (Llobera, 2001). This index ranges from −1 in lower landscape positions (within a user-defined search radius) to 1 in higher landscape positions. Due to the differences in landform size between the two catenas, this index was computed using a 50-m search radius at SJER and a 100-m search radius at SFREC.

Daily estimates of beam radiation were modeled with the ESRA solar radiation model (Rigollier et al., 2000), and summed to generate an annual beam radiance surface. A constant Linke turbidity (Kasten, 1996) representative of the study sites (T_L = 3.0) was used to partition beam from diffuse radiance. Output from the ESRA model is an effective index of microclimate in this region, integrating slope angle, slope aspect, and shading from adjacent terrain (Beaudette and O'Geen, 2009).

Distributions of select terrain attribute values in each catena (annual beam radiance, CTI, and mean curvature) were extracted at soil profile locations and compared with corresponding distributions derived from entire raster surfaces. Visual inspection of box and whisker plots confirmed that there was generally good agreement between distributions of terrain attribute values extracted at soil profile locations and distributions from entire catenas (Fig. 2). Sampled sites were slightly biased towards landscape positions receiving more annual beam radiance (more so at SJER), and to concave surfaces (more so at SJER) (Fig. 2). Differences between the shape and central tendency of distributions are expected to contribute some bias to the statistical models developed. The truncated distributions associated with values extracted at soil profile locations limit our ability to extrapolate across the full range of the terrain attributes within each catena.

Statistical Analysis

Spearman rank correlation coefficients were used to gauge the sign and magnitude of relationships between terrain-shape indices and measurements of soil moisture. Spearman's rank correlation coefficient (r_s) is a rank-based metric used in cases when nonlinear, but strictly monotonic, relationships are hypothesized (Verzani, 2004). Partial Spearman rank correlation coefficients were computed to adjust for mutual correlation among terrain-shape indices, measured soil moisture, and weighted-mean particle diameter (WMPD):

$$r_{12.3} = \frac{r_{12} - r_{13}r_{23}}{\sqrt{1-r_{13}^2}\sqrt{1-r_{23}^2}} \quad [2]$$

where $r_{12.3}$ is the partial Spearman correlation coefficient between Variable 1 and 2, after adjusting for Variable 3. The parameters r_{12}, r_{13}, and r_{23} are the Spearman correlation coefficients between Variables 1 and 2, 1, and 3, and 2 and 3, respectively (Legendre and Legendre, 1998).

Collinearity within all models was evaluated with the variance inflation factor (VIF):

$$\mathrm{VIF}_i = \frac{1}{\left(1 - R_i^2\right)} \quad [3]$$

where VIF_i is the variance inflation factor for variable i and R_i^2 is the coefficient of determination when variable i is regressed on

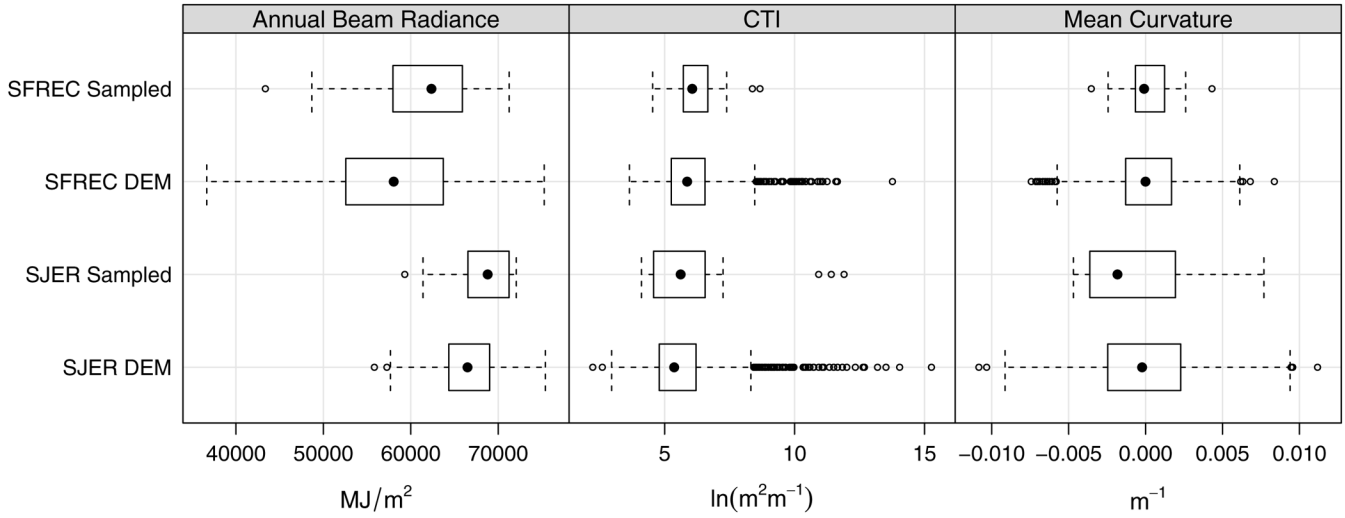

Fig. 2. Digital elevation model (DEM)-derived terrain attribute distributions from soil profile locations and catena-wide rasters. Box and whisker plots represent sample medians (filled circles), inter-quartile range (boxes), 1.5 times the value of the first or third quartile (whiskers), and values outside the range defined by the whiskers (open circles).

all other predictors (Harrell, 2001). All models described within this study had VIF values between 1 and 3, suggesting that collinearity was not large enough to confound interpretation of partial explained variances, coefficients, or standard errors.

Seven post-rainfall periods (PRP) were selected as a basis for comparisons between DEM-derived terrain shape indices and measured soil moisture (Fig. 3, Supplemental Fig. 1 and 2). This style of analysis was selected based on the observations that: (i) volumetric water content typically decreased linearly after each rain event; (ii) the slope and mean water content within each PRP have a direct interpretation; and, (iii) a simple linear modeling framework could be used for analysis. The PRP numbers 1 to 2 are representative of the early winter wet-up phase, numbers 3 to 4 representative of the winter wet phase, and numbers 5 to 7 representative of the dry-down (spring utilization) phase. Within each PRP, a linear model was fit to the soil moisture data (by sensor) such that model intercepts described soil moisture values at the midpoint of each PRP and model slopes described rates of soil moisture change through the duration of the PRP (Fig. 3). Fitted intercepts can be interpreted as PRP-wise mean VWC, and are denoted as $\overline{\text{VWC}}$. Likewise, fitted slopes are interpreted as either PRP-wise wet-up rates (positive change in VWC per day) or PRP-wise dry-down rates (negative change in VWC per day), and are denoted as ΔVWC. Multiple linear regression was used to determine the partial variance in $\overline{\text{VWC}}$ and ΔVWC explained by beam radiance, CTI, WMPD, and canopy cover (SFREC only) within each PRP. Regression models were fit for each sensor depth (10, 30, and 50 cm) and within each PRP. Canopy cover (SFREC only) was determined in the field and converted into a categorical variable describing observations as either: closed canopy, partial canopy, or open canopy. Of the many terrain-shape indices compared in this paper, CTI was selected for the variance partitioning component of analysis due to the fact that it is one of the most widely applied indices of water

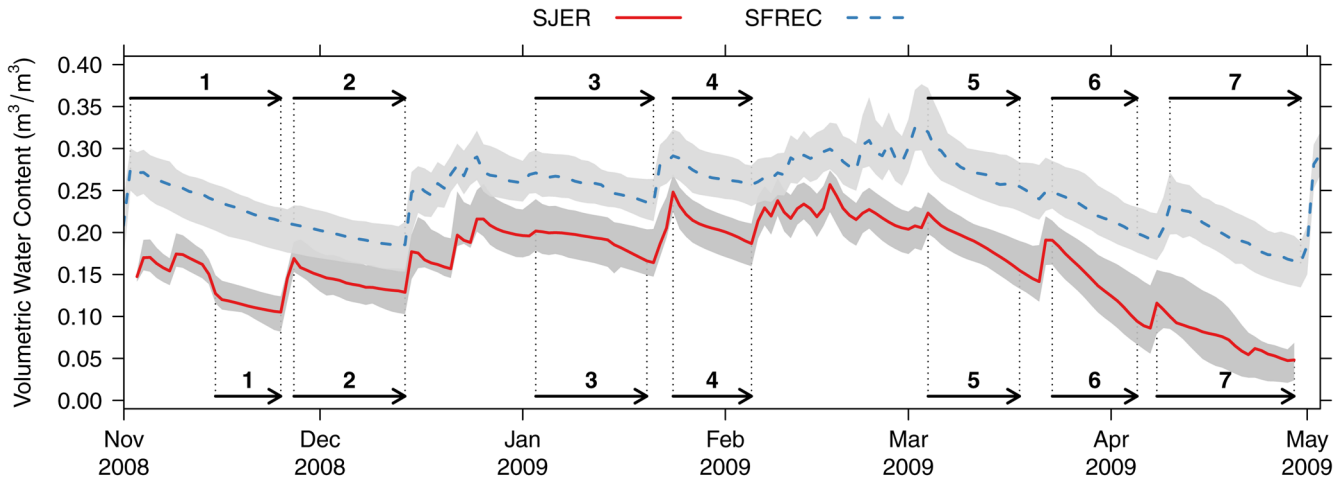

Fig. 3. Daily median soil moisture values at 10 cm. Shaded regions represent 25th and 75th percentile soil moisture values, and illustrate spatial variability at each time step. Peaks track occurrence of rainfall events. Post-rainfall periods (PRPs) represent periods between storm events and are delineated by vertical dotted lines, PRPs 1 to 2 occur during a phase when dry soils are being recharged, PRPs 3 to 4 occur during a phase when soils are at or near saturation, and PRPs 5 to 7 occur during a utilization phase.

and sediment redistribution. Partial effects (i.e., partial slopes) and corresponding standard errors were used to describe temporal changes in sign, magnitude, and statistical significance of CTI and beam radiance.

RESULTS AND DISCUSSION

Soil Properties

Soil depth at SJER ranged from shallow (<50 cm) to very deep (>150 cm), with lithic or paralithic contact typically occurring near 80 to 90 cm. At summit positions, soils were generally shallow with loamy particle size classes when bedrock was closer in composition to granite, while soils formed on granodiorite or diorite were moderately deep and coarse-loamy. In swale positions, soils were very deep and coarse-loamy, but fine-loamy in swales found at the base of landforms where bedrock was predominately diorite. Soils on backslopes were typically moderately deep to deep, and coarse-loamy, regardless of bedrock composition. Cambic and weak argillic horizons were common, typically with little evidence of clay illuviation and iron oxide production (10YR hues) (Table 1). Evidence of more soil development was present in soils formed from dioritic residuum and colluvium, with greater clay production, redder hues (7.5YR), and greater occurrence of clay films.

Soil depth at SFREC ranged from shallow to deep, with lithic or paralithic contact typically occurring near 80 to 90 cm. Soil textures were generally loamy-skeletal or fine-loamy, having few clear patterns with respect to landscape position. Most profiles had thick argillic horizons (20–70 cm) with abrupt or clear horizon boundaries, nearly 100% of ped faces had distinct clay films, bright red colors (5YR to 2.5YR hue and chroma of 4–6) as well as an absolute increase in clay content relative to overlying horizons of 10 to 25% (Tables 1 and 2). Profile development at SFREC did not follow clear relationships with regards to landscape position, however, more developed soils coincided with areas of bedrock having higher iron content (data not shown).

Weighted-mean particle diameter (WMPD) was used as a proxy for water-holding capacity, based on the assumption that WMPD values were inversely, monotonically, and approximately linearly related to water-holding capacity. It should be noted that WMPD values do not account for differences in water-holding capacity that are driven by other factors such as organic matter content, rock fragment content, compaction, or soil structure. The WMPD values ranged from 0.30 to 0.61 mm at SJER and from 0.05 to 0.49 mm at SFREC (Table 2). Median WMPD values were typically three times larger at SJER as compared to SFREC at 10-, 30-, and 50-cm depths (Table 3). Site-wide variation in WMPD was fairly consistent with depth at SJER (0.064–0.075 mm inter-quartile range), and generally 1.5 to 2 times greater than corresponding site-wide variation in WMPD at SFREC (Table 3). In contrast, site-wide variation in WMPD varied greatly (0.039–0.068 mm inter-quartile range) with depth at SFREC. Differences in WMPD variability with depth mirror the relative differences in profile development found at each study site.

Soil Moisture

At SJER, soil moisture content (θ_v) near the surface was consistently greater than at depth during the early winter wet-up phase (PRP 1–2: November though late December), approximately equal through the winter-wet phase (PRP 3–4: mid-January through March), and consistently lower during the spring (PRP 5–7: March through May) dry-down phase (Fig. 4).

Table 1. Representative soil morphologic data from each study site, from selected soil profile descriptions. Soil profile "007" from the San Joaquin Experimental Range (SJER-granitic lithology) was sampled on a north-facing backslope and is classified as coarse-loamy, mixed, superactive, thermic Typic Haploxerept. Soil profile "N35" from the Sierra Foothill Research and Extension Center (SFREC-metavolcanic lithology) was sampled on a northwest-facing backslope and is classified as fine-loamy, mixed, superactive, thermic Mollic Haploxeralf.

Site	Horizon	Depth	Boundary†	Color		Structure‡	Consistence§	>2 mm	Texture¶
				Dry	Moist				
		cm						%	
SJER (007)	A	0–5	AW	10YR 5/3	10YR 4/3	1 F SBK	VFR, SS, PO	7	COSL
	AB1	5–22	GW	10YR 5/2	10YR 4/2	2 M SBK	FR, SS, PO	7	COSL
	AB2	22–45	GW	10YR 5/2	10YR 4/2	2 CO SBK	FR, SS, PO	7	COSL
	Bw1	45–65	CW	10YR 6/3	10YR 4/2	2 M ABK	FR, SS, PO	10	COSL
	Bw2	65–80	CI	10YR 7/3	10YR 5/2	MA	FR, MS, SP	10	COSL
	R	80+	–	–	–	–	–	–	–
SFREC (N35)	A	0–10	CW	7.5YR 5/6	7.5YR 3/4	1 M SBK	VFR, SS, SP	10	L
	BA	10–26	CW	5YR 5/6	5YR 3.5/4	2 CO ABK	FR, MS, MP	10	L
	Bt1	26–53	AW	5YR 4.5/6	5YR 3.5/5	2 M ABK	FR, MS, VP	15	GRL
	2Bt2	53–72	AW	7.5YR 4/4	7.5YR 4/4	3 CO ABK	SR, MS, VP	20	CBCL
	2Bt/Crt	72–88	CW	2.5YR 4/3	2.5YR 4/3	1 F ABK	SR, MS, VP	25	CBCL
	R	88+	–	–	–	–	–	–	–

† Boundary: AW = abrupt wavy, GW = gradual wavy, CW = clear wavy, CI = clear irregular.

‡ Structure: F = fine, M = medium, CO = coarse, SBK = sub-angular blocky, ABK = angular blocky, MA = massive.

§ Consistence: VFR = very friable, FR = friable, SR= slightly rigid, SS = slightly sticky, MS = moderately sticky, PO = not plastic, SP = slightly plastic, MP = moderately plastic, VP = very plastic.

¶ Texture: COSL = coarse sandy loam, L = loam, GRL = gravelly loam, CBCL = cobbly clay loam.

Table 2. Particle-size distribution for representative soils from each study site. Sand fraction classes correspond to limits defined by the USDA.

Site	Horizon	Clay	Silt	Total sand	VCS†	CS‡	MS§	FS¶	VFS#	WMPD††
		%								mm
SJER‡‡ (007)	A	8	16	76	12	22	12	21	10	0.44
	AB1	7	16	77	12	21	10	23	11	0.42
	AB2	7	16	77	13	20	12	21	11	0.44
	Bw1	8	16	76	12	22	11	22	11	0.43
	Bw2	9	16	75	11	20	11	22	11	0.40
SFREC (N35)	A	15	41	44	7	9	6	12	11	0.24
	BA	19	41	40	5	7	5	12	11	0.19
	Bt1	26	36	38	7	6	5	10	11	0.21
	2Bt2	35	32	33	5	4	3	11	10	0.15
	2Bt/Crt	39	27	34	10	5	3	8	8	0.22

† VCS = very coarse sand.

‡ CS = coarse sand.

§ MS = medium sand.

¶ FS = fine sand.

VFS = very fine sand.

†† WMPD = weighted mean particle diameter.

‡‡ SJER = San Joaquin Experimental Range; parent material derived from granitic rocks; SFREC = Sierra Foothill Research and Extension Center; parent material derived from metavolcanic rocks

This pattern is typical of most freely drained soils where the soil profile "fills" from the top-down at the onset of the winter rainy season, remains at or above field capacity during the peak of the rainy season, and "empties" from the top-down during spring and early summer. Once soil profiles at SJER reached field capacity (PRP 4), θ_v measured at 10-, 30-, and 50-cm depths were similar. This was likely due to the relatively low degree of soil profile development at SJER, with clear and gradual horizon boundaries and little change in soil texture (and therefore water-holding capacity) over depth. Site-wide median WMPD values were consistent over the three depths where soil moisture was measured: 0.47 mm WMPD at 10 cm, 0.45 mm at 30 cm, and 0.44 mm at 50 cm. Water content measured at 10 cm was consistently more temporally and spatially variable than at 30- and 50-cm depths due to rapid infiltration, percolation, and loss to evapotranspiration (Fig. 4).

At SFREC, θ_v at 10 cm was only greater than measurements collected from 30- and 50-cm depths during the initial wet-up phase (PRP 1–2: November through mid-December). During the late wet-up (PRP 3: January), winter-wet (PRP 4: February), and dry-down (PRP 5–7: mid-March through May) phases, θ_v at 10 cm was consistently lower than measurements collected from 30 and 50 cm. Higher water-holding capacity in the BA and Bt horizons, coupled with near-surface water use by annual grasses were probably responsible for the strong vertical differentiation in soil moisture. Annual grass roots are typically confined to the upper 10 cm of soil in early March through April, and ultimately extend to a maximum of about 30 cm at maturity (Gordon and Rice, 1992; Holmes and Rice, 1996). At 10 and 30 cm, θ_v converged during the first major rainfall event in 2008 (November), and exceeded θ_v at 50 cm during the second major rainfall event in 2008 (Fig. 5). From January 2009, θ_v at 50 cm steadily increased through the rainy season until becoming recharged to field capacity in early March 2009 (Fig. 5). By PRP 3, θ_v was greatest at 50 cm, and decreased with proximity to the soil surface. This was likely due to the strong degree of soil development at SFREC, partially expressed as abrupt and clear horizon boundaries and strong vertical differentiation of soil texture (and water-holding capacity). Soil textures at 10 cm were typically loams, while textures at 30 and 50 cm were clay loams. During spring (March–June), soil moisture was rapidly lost between rainfall events, with the greatest rates of dry-down near the surface. The timing of annual grass growth and blue oak bud break (early March) coincided with increased steepening of

Table 3. Weighted mean particle diameter (WMPD) values, summarized by site and sensor depth. Spread around the median and mean is given as the inter-quartile range (IQR) and standard deviation (SD).

Site	Depth	Minimum	First quartile	Median	Mean	Third quartile	Maximum	IQR	SD
	cm	mm							
SJER†	10	0.36	0.43	0.47	0.47	0.51	0.63	0.075	0.072
SJER	30	0.35	0.43	0.45	0.46	0.50	0.60	0.064	0.065
SJER	50	0.31	0.42	0.44	0.46	0.49	0.61	0.072	0.078
SFREC	10	0.06	0.15	0.17	0.18	0.19	0.35	0.039	0.050
SFREC	30	0.08	0.12	0.15	0.15	0.17	0.43	0.053	0.053
SFREC	50	0.07	0.11	0.14	0.15	0.17	0.49	0.068	0.077

† SJER = San Joaquin Experimental Range; SFREC = Sierra Foothill Research and Extension Center.

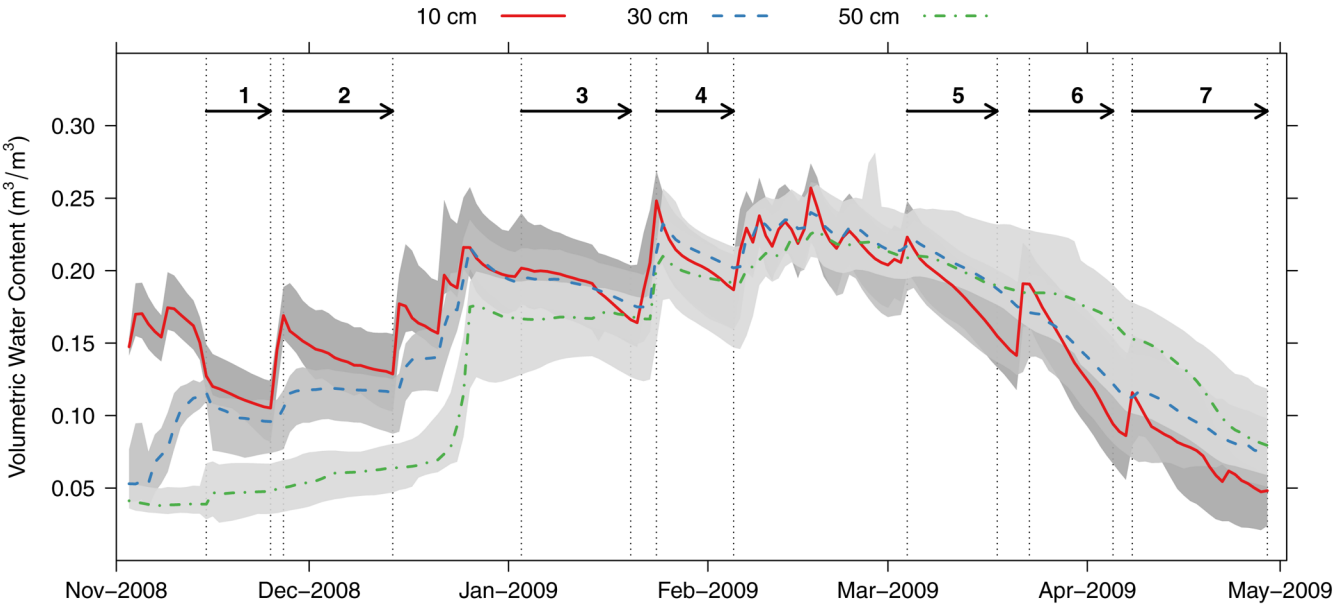

Fig. 4. Site-wide median soil moisture values at San Joaquin Experimental Range (SJER), aggregated by day and sensor depth. Shaded regions represent 25th and 75th percentile soil moisture values, and illustrate spatial variability at each time step. Peaks track occurrence of rainfall events. Post-rainfall periods (PRPs) represent periods between storm events and are delineated by vertical dotted lines, PRPs 1 to 2 occur during a phase when dry soils are being recharged, PRPs 3 to 4 occur during a phase when soils are at or near saturation, and PRPs 5 to 7 occur during a utilization phase.

dry-down rates observed between March and May 2009 (Fig. 5). The similar dry-down rates at 30 and 50 cm were likely due to similar water-holding capacity (estimated via WMPD; Table 3) and utilization by deeper-rooted oak and pine species as opposed to annual grasses.

Temporal Stability of Terrain-Shape Indices

A sequence of partial Spearman correlation coefficients was used to construct a temporal matrix of how well selected terrain-based proxies were correlated with $\overline{VWC}$ (mean volumetric water content) and ΔVWC (change in volumetric water content) (Fig. 6). Terrain-based proxies were generally better predictors of ΔVWC as compared to $\overline{VWC}$ (both sites), and correlations were always greater at SJER compared to SFREC (Fig. 6). However, no single terrain-based proxy showed a high level of consistency in terms of correlation with $\overline{VWC}$ or ΔVWC over time, across depth, or between sites. It should be noted that many of these proxies were highly correlated with each other, and therefore

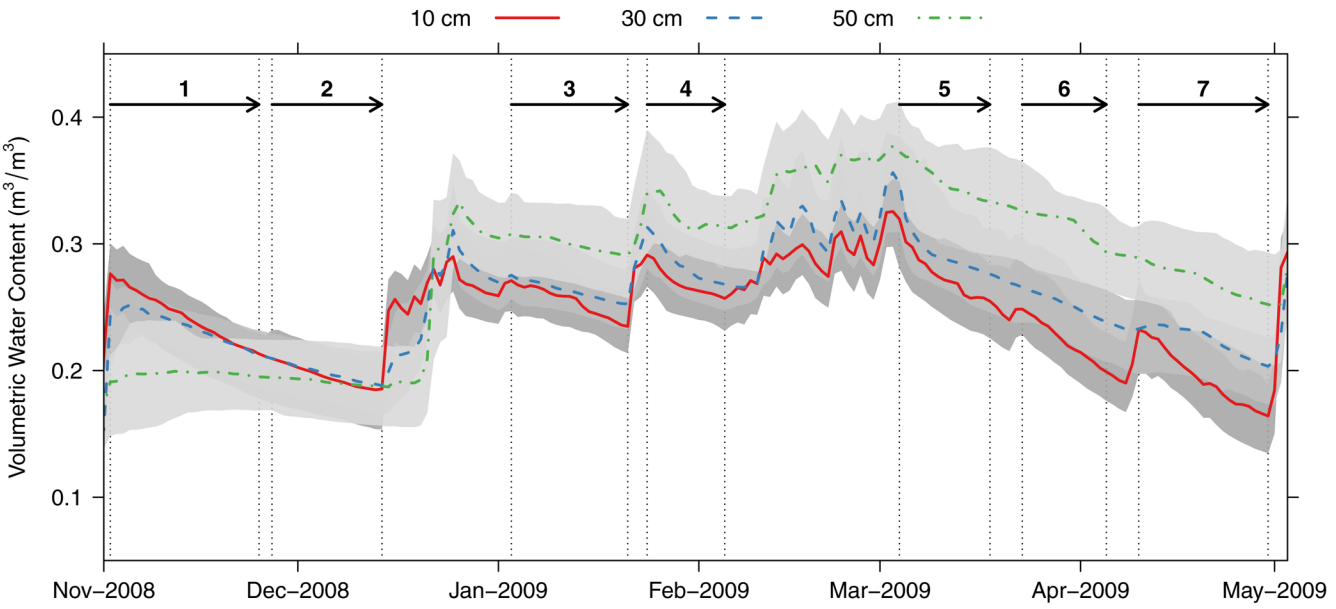

Fig. 5. Site-wide median soil moisture values at Sierra Foothill Research and Extension Center (SFREC), aggregated by day and sensor depth. Shaded regions represent 25th and 75th percentile soil moisture values, and illustrate spatial variability at each time step. Peaks track occurrence of rainfall events. Post-rainfall periods (PRPs) represent periods between storm events and are delineated by vertical dotted lines, PRPs 1 to 2 occur during a phase when dry soils are being recharged, PRPs 3 to 4 occur during a phase when soils are at or near saturation, and PRPs 5 to 7 occur during a utilization phase.

much of the information regarding terrain shape is shared among proxies. For example, slope gradient (GRAD) and PCURV were moderately correlated with each other at both catenas (r_s = 0.2–0.4), and TCI, CTI, MCURV, TCURV, and PROM were highly correlated with each other at both catenas (r_s = 0.5–0.9). However, this correlation structure was not always apparent in the temporal fluctuation of partial correlation between measured soil moisture and terrain-shape proxies (Fig. 6).

At SJER, correlation between $\overline{\text{VWC}}$ and terrain-based proxies was generally greatest at 30 cm. The dominant predictors of $\overline{\text{VWC}}$ varied by depth, with MCURV and TCI performing the best at 10 and 30 cm, and GRAD performing the best at 50 cm (Fig. 6). The temporal stability of these correlations (i.e., the consistency of dominant predictors of $\overline{\text{VWC}}$ across all PRP) was greatest at 30 and 50 cm, with a maximum correlation at PRP 5 and 6. Correlation between ΔVWC and terrain-based proxies was generally greatest during PRP 1 and 2 at 10 cm, PRP 3, 5, and 6 at 30 cm, and PRP 5, 6, and 7 at 50 cm. The CTI, TCURV, and PROM were the best performing proxies for ΔVWC (Fig. 6). As is the case in other studies, correlation between soil moisture dynamics and terrain attributes appears to be stronger in landscapes where soil profile variability is uniform. In a study having pronounced wet and dry seasons, elevation, slope, and distance to stream channels were the best predictors of soil wetness (Campling et al., 2002). The accuracy of prediction decreased, however, when comparing landscape positions that were increasingly well drained. A diminished capacity to predict soil moisture variability at broader scales was also observed by Park and van de Giesen (2004). They were able to increase their ability to explain soil moisture variability with terrain attributes by stratifying the landscape into hydrologic landscape units, which effectively reduced the spatial variation of soil moisture across a given portion of the landscape.

At SFREC, correlation between $\overline{\text{VWC}}$ and terrain-based proxies was greatest at 30- and 50-cm depths, however, the magnitude of correlations was low (0.0 < r_s < 0.3) (Fig. 6). Slope

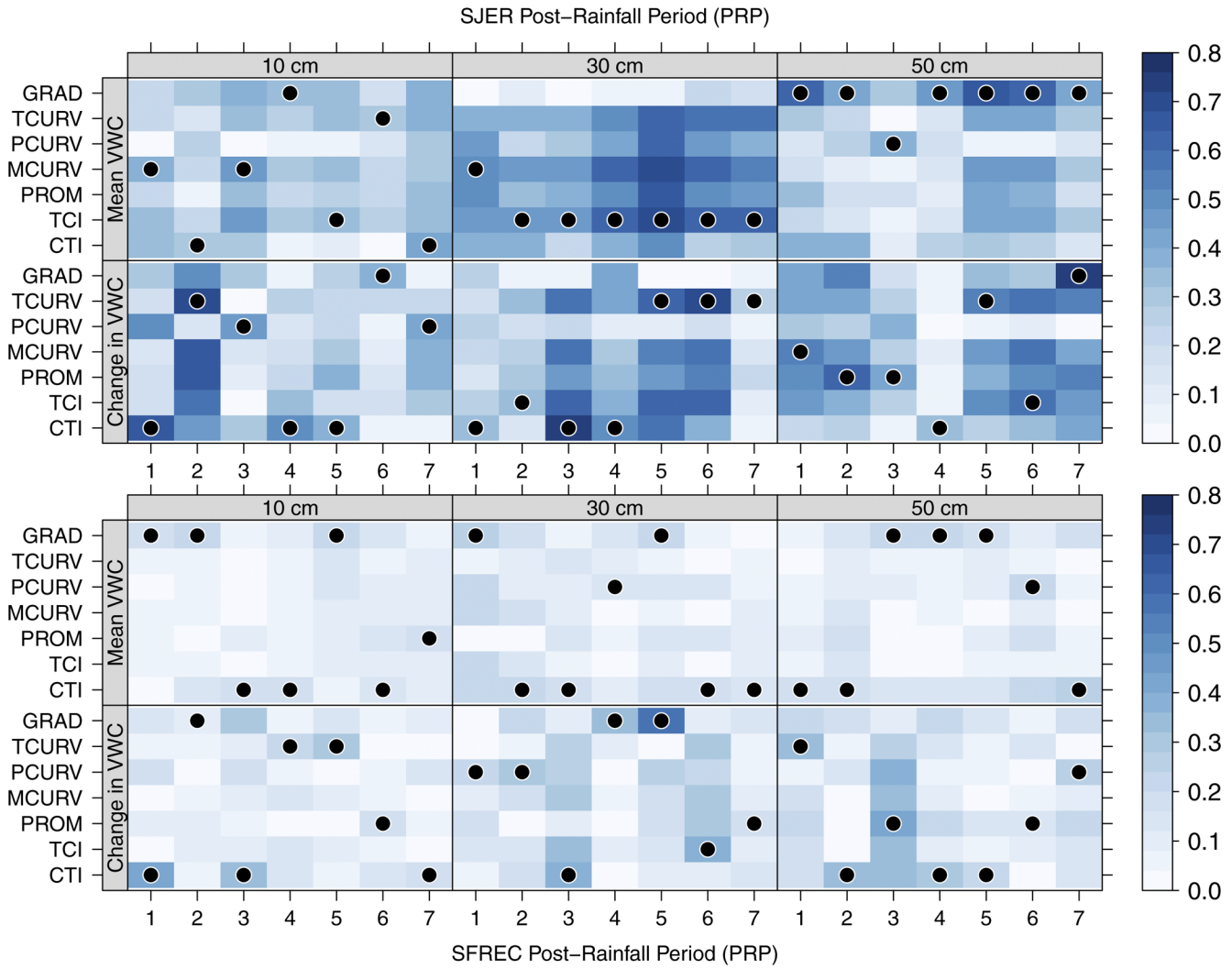

Fig. 6. Partial Spearman correlation coefficients (absolute value) computed from terrain-shape indices and post-rainfall period (PRP)-wise mean volumetric water content ($\overline{\text{VWC}}$) and change in volumetric water content (ΔVWC), after removing correlation with weighted mean particle diameter (WMPD) at (a) San Joaquin Experimental Range (SJER) and (b) Sierra Foothill Research and Extension Center (SFREC). Filled symbols have been placed in cells corresponding to the terrain-shape index with the highest partial correlation to $\overline{\text{VWC}}$ and ΔVWC. Terrain-shape indices have been abbreviated as: slope (GRAD), tangential curvature (TCURV), profile curvature (PCURV), mean curvature (MCURV), topographic prominence (PROM), terrain characterization index (TCI), and compound topographic index (CTI).

gradient (GRAD) and CTI where the best performing proxies across PRP and depth. Temporal stability of correlations was slightly greater at 30 cm, as compared to 10 and 50 cm, however, the differences were small. Correlation between ΔVWC and terrain-based proxies was approximately equivalent across depths, with CTI and GRAD performing best (Fig. 6).

It is plausible that temporal stability and dominance of partial correlation coefficients presented in Fig. 6 are related to processes that control the scale of spatial variability of $\overline{\text{VWC}}$ at SJER. For example, bioturbation, micro-topographic variation, subsurface lateral flow and complex patterns in vegetation type and density likely give rise to heterogeneous patterns in soil moisture near the soil surface and in the rooting zone of annual grasses and forbes (approximately 10 cm in March and April); possibly explaining the low degree of temporal stability in any given proxy's ability to predict $\overline{\text{VWC}}$. Studies have shown that the spatial distribution of soil moisture content becomes highly organized and correlated with terrain parameters, such as upslope contributing area, when the catchment is at or near saturation (Western and Blöschl, 1999; Western et al., 1999). Other studies have demonstrated increased spatial variability in soil moisture as soils in the catchment are recharged (Owe et al., 1982). High variability during wet periods was attributed to the combination of well-drained soils and steeply sloping terrain in Pennsylvania (Takagi and Lin, 2011). Moreover, studies have shown that hydrologic flowpaths change over time from vertical infiltration during wet-up to subsurface lateral flow at or near saturation causing redistribution of moisture across the landscape (Redding and Devito, 2008; Rains et al., 2006; Swarowsky et al., 2012).

The larger magnitude in correlation coefficients and the high degree of temporal stability observed deeper in the soil profile (>30 cm) may be related to more homogenous conditions affecting soil moisture–particularly during the end of the winter-wet phase and beginning of the spring dry-down phase (PRP 4 and 5). Temporally stable soil moisture conditions in deeper horizons were also observed in sloping terrain in the Shale Hills catchment in central Pennsylvania (Takagi and Lin, 2011). The fact that TCI (an integrated measure of surface curvature and upslope contributing area) was the best predictor of $\overline{\text{VWC}}$ at 30-cm depth, suggests that spatial patterns in soil moisture likely extend over greater distances at 30 cm, as compared to 10 or 50 cm. The dominance and temporal stability of slope as a predictor of $\overline{\text{VWC}}$ at 50 cm suggests that distances over which spatial patterns in soil moisture exist are likely to lie somewhere between shorter-distance patterns at 10 cm, and longer-distance patterns at 30 cm. Such scales may reflect complexity in bedrock topography and weathered bedrock permeability, which have been found to influence soil moisture variability (Tromp-van Meerveld and McDonnell, 2006; Tromp-van Meerveld et al., 2007). Stratigraphic relationships among soil profiles and horizons such as the presence of Bt horizons, clay content, and distinctness and topography of horizon boundaries also influence soil moisture variability (Swarowsky et al., 2011, 2012).

The vertical "stripes" within Fig. 6 are associated with temporally changing conditions that cause entire suites of terrain-shape attributes to rapidly oscillate from low to high partial Spearman correlation (r_s) with respect to either $\overline{\text{VWC}}$ or ΔVWC. Sudden increases in r_s could be caused by θ_v reaching a critical threshold (e.g., saturation) that enhances spatial organization of soil moisture at scales comparable to terrain-shape attributes (Burt and Butcher, 1985). Some examples of these sudden increases in r_s occur within the SJER catena at PRP 2 (10 cm), 4 (30 cm), and 5 (50 cm) for $\overline{\text{VWC}}$ and at PRP 2 (10 cm), 3 (30 cm), and 5 (50 cm) for ΔVWC (Fig. 6). While much less pronounced, sudden increases in r_s occur within the SFREC catena at PRP 5 (10 cm) and 2 (50 cm) for $\overline{\text{VWC}}$, and at PRP 3 (10, 30, and 50 cm) for ΔVWC (Fig. 6). Large negative changes in r_s between PRPs may be attributed to either loss of sufficient soil moisture to support spatial organization, or conditions where soil texture, macropore drainage, ET, or some other parameter was the dominant factor controlling spatial patterns in θ_v.

Partitioning Variance in Soil Moisture

At SJER, total explained variance in $\overline{\text{VWC}}$ by solar radiation, CTI, and WMPD, within a single PRP, and at a single depth was greatest near the soil surface and generally decreased with depth (Fig. 7). Partial variance in $\overline{\text{VWC}}$ was largely explained (30–70% of total) by modeled beam radiance and CTI at 10-cm depth, moderately explained by CTI (15–40% of total) at 30-cm depth, and weakly to moderately explained by a combination of CTI, modeled beam radiance and WMPD (20–40% absolute) at 50 cm (Fig. 7). Partial variance in $\overline{\text{VWC}}$ explained by modeled beam radiance (5–25% absolute) and CTI (15–50% absolute) was greatest near the surface (10 cm) and during the early winter wet-up (PRP 1 and 2) phases. At 30 cm, CTI was the best predictor of $\overline{\text{VWC}}$, and explained increasing amounts of variance from PRP 1 (15% absolute) to PRP 7 (36% absolute). Partial variance explained by WMPD was low overall, but greatest at 50 cm (2–10% absolute). The relatively weak predictive power of WMPD was likely due to the homogeneity of soil texture and infrequent occurrence of argillic horizons at SJER (Tables 2 and 3). The timing of maximum partial variance explained by WMPD (wet-up and dry-down) corresponds to times when soil water potential (not measured) was likely within the window of water potential (10–100 kPa) where maximum correlation between particle size distribution and soil water content has been described (Pachepsky et al., 2001).

These patterns suggest that spatial variability of $\overline{\text{VWC}}$ landscapes similar to SJER is most readily predicted via terrain and microclimate proxies near the soil surface and during the wet-up and dry-down phases of the water year. In addition, differences in water-holding capacity (as expressed in terms of WMPD) explained (marginally) more partial variance in $\overline{\text{VWC}}$ with depth. Mirroring trends in the temporal stability of partial correlation between $\overline{\text{VWC}}$ and terrain-based proxies (Fig. 6), temporal stability in partial variance explained was greatest at 30 cm.

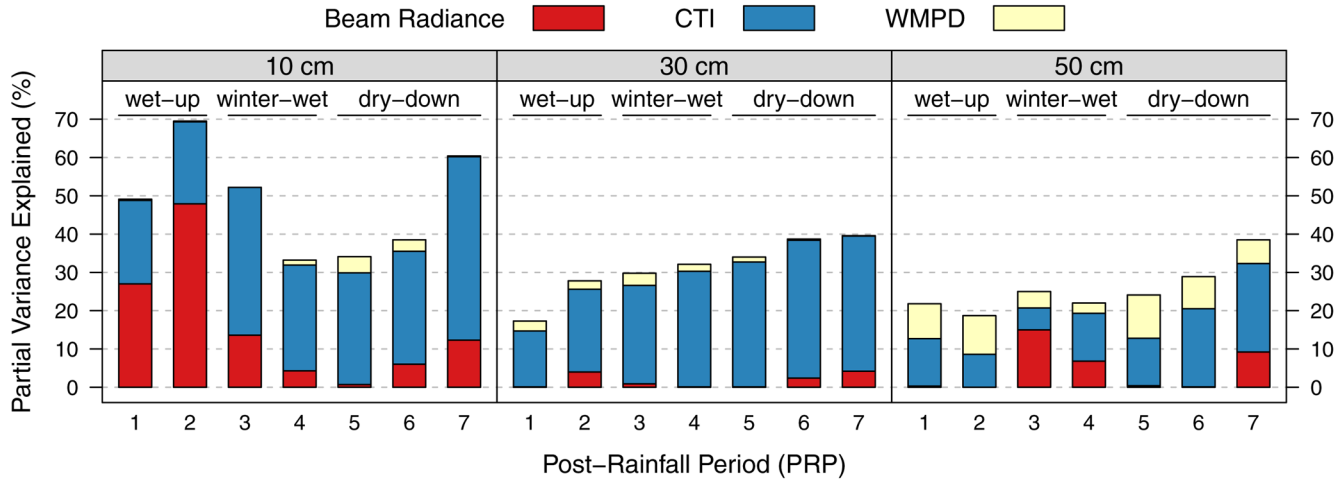

Fig. 7. Partial variance in mean volumetric water content ($\overline{VWC}$) at San Joaquin Experimental Range (SJER) explained by beam radiance, compound topographic index (CTI), and weighted mean particle diameter (WMPD), by post-rainfall periods (PRP) and sensor depth. Partial variances sum to approximately the total variance explained by multiple regression.

In contrast to SJER, total explained variance in $\overline{VWC}$ was generally low (20–40% at 30 cm) to very low (2–20% at 10 and 50 cm) at SFREC (Fig. 8). Partial explained variance in $\overline{VWC}$ was mainly accounted for by a combination of WMPD and canopy cover, with CTI and modeled beam radiance accounting for <10%. The small amount of partial variance in $\overline{VWC}$ explained by modeled beam radiance was greatest during the spring dry-down phase (PRP 5, 6, 7). Partial variance explained by CTI was greatest during the winter wet-phase at 10 and 30 cm, and during the wet-up phase at 50 cm. These patterns suggest that in landscapes similar to SFREC, spatial variation in $\overline{VWC}$ is probably controlled by differences in water-holding capacity among horizons and vegetation density; as well as factors that were not explicitly modeled: soil structure, macroporosity, perched water tables, abrupt textural changes, etc.

At SJER, total explained variance in ΔVWC varied widely across depths and PRP (Fig. 9). Near the surface (10 cm), modeled beam radiance explained the largest proportion of total variance during the spring dry-down phase (PRP 6 and 7), while CTI explained the largest proportion of total variance during the early winter wet-up phase (PRP 1 and 2). This shift in the dominance of beam radiance vs. CTI was likely caused by seasonal changes in landscape processes that control rates of soil moisture redistribution and utilization (Swarowsky et al., 2011). In fall wet-up months (PRP 1 and 2), annual grasses and forbes that typically use most of the soil moisture in the top 10 to 15 cm of soil are just germinating; resulting in a gravitational gradient-controlled redistribution of soil moisture (i.e., dominance of partial variance explained by CTI). In the late spring dry-down phase (PRP 6 and 7), rapid growth of annual grasses and forbes, coupled with the low water-holding capacity of surface horizons, likely results in evapotranspiration-controlled redistribution rates (i.e., the dominance of partial variance explained by beam radiance). At 30 cm, CTI was always the best predictor of ΔVWC, explaining the largest proportion of partial variance during the spring dry-down phase (PRP 5, 6, 7). The CTI and modeled beam ra-

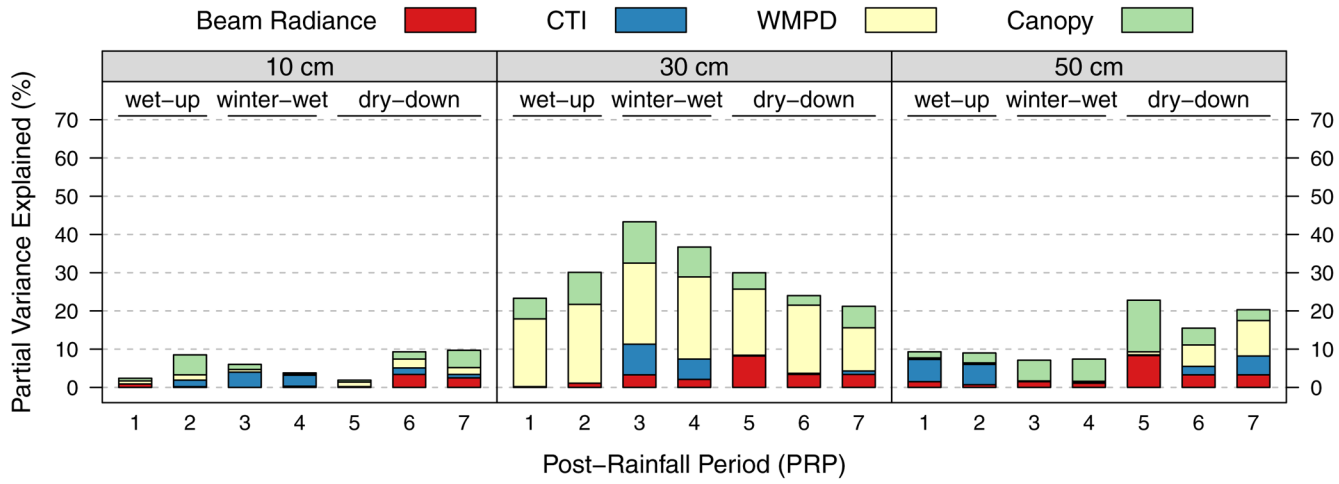

Fig. 8. Partial variance in mean volumetric water content ($\overline{VWC}$) at Sierra Foothill Research and Extension Center (SFREC) explained by beam radiance, compound topographic index (CTI), weighted mean particle diameter (WMPD), and canopy cover, by by post-rainfall periods (PRPs) and sensor depth. Partial variances sum to approximately the total variance explained by multiple regression.

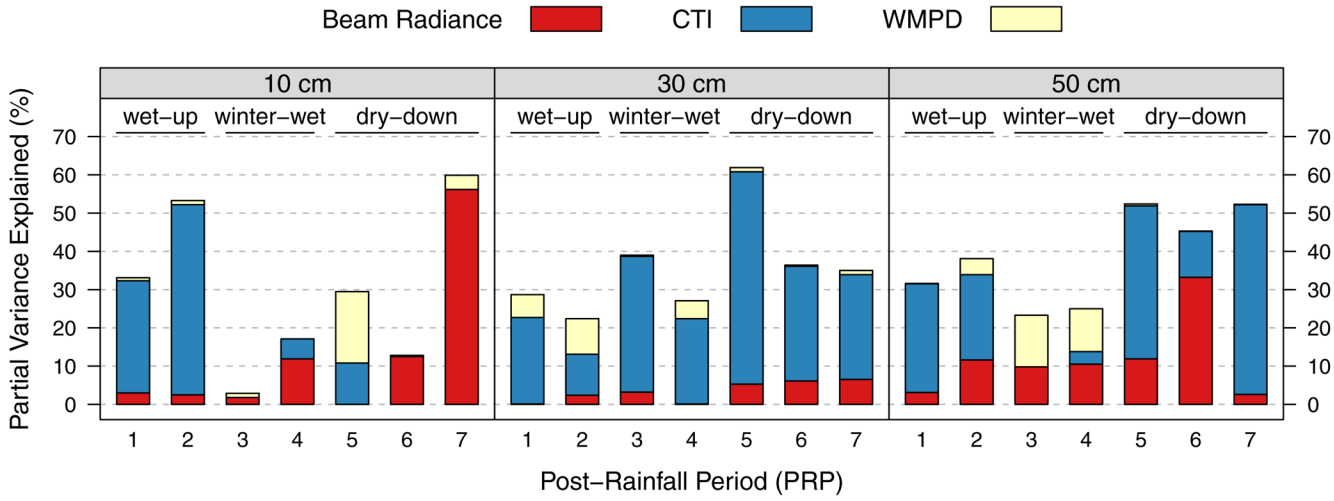

Fig. 9. Partial variance in change in volumentric water content (ΔVWC) at San Joaquin Experimental Range (SJER) explained by beam radiance, compound topographic index (CTI), and weighted mean particle diameter (WMPD), by post rainfall periods (PRPs) and sensor depth. Partial variances sum to approximately the total variance explained by multiple regression.

diance accounted for a greater proportion of the total variance explained in ΔVWC at 30 and 50 cm, as compared to their predictive capacity in terms of $\overline{\text{VWC}}$. This may have been due to the fact that rates of soil moisture change at depth are somewhat "insulated" from processes that affect soil moisture utilization near the surface at the meter to centimeter scale (i.e., less predictable), and therefore are more likely to be controlled by gravitational gradients and possibly vegetation density operating over 10s to 100s of meters. Partial variance explained by WMPD was generally greatest (5–20%) during the winter-wet phase and the beginning of the spring dry-down phase. The WMPD was a relatively better predictor of partial variance in ΔVWC than $\overline{\text{VWC}}$ at SJER. This suggests that post-rainfall dry-down rates (ΔVWC) in these landscapes are more affected by differences in WMPD compared to post-rainfall average soil moisture ($\overline{\text{VWC}}$).

At SFREC, total explained variance in ΔVWC was greatest near the surface (10–35%), with the largest proportion of partial variance explained by canopy cover (Fig. 10). The greater importance of canopy cover at 10 and 30 cm may be related to differences in soil moisture utilization by understory vs. inter-canopy species (Jackson et al., 1990). Thicker A horizons, higher organic matter content, and larger structural units associated with soils found under tree canopies in this type of ecosystem coupled with an estimated 27% canopy interception rate (Dahlgren et al., 1997) likely contributed to variance explained by the canopy cover variable. Near the soil surface (10 cm), CTI accounted for a small amount (5–10%) of the total variance during the beginning of the wet-up phase (PRP 1) and end of the spring dry-down phase (PRP 7), whereas beam radiance accounted for 8 to 15% during the winter-wet phase (PRP 3 and 4). At 50 cm, CTI accounted for 5 to 20% of the total variance in ΔVWC during the end of the wet-up and for the duration of the winter-wet phases. The small shift in dominance from beam radiance near the soil surface (10 cm) to CTI at depth (50 cm), tracks expected dominance of processes affecting soil moisture redistribution: evapotranspiration demand near the surface and lateral flow at

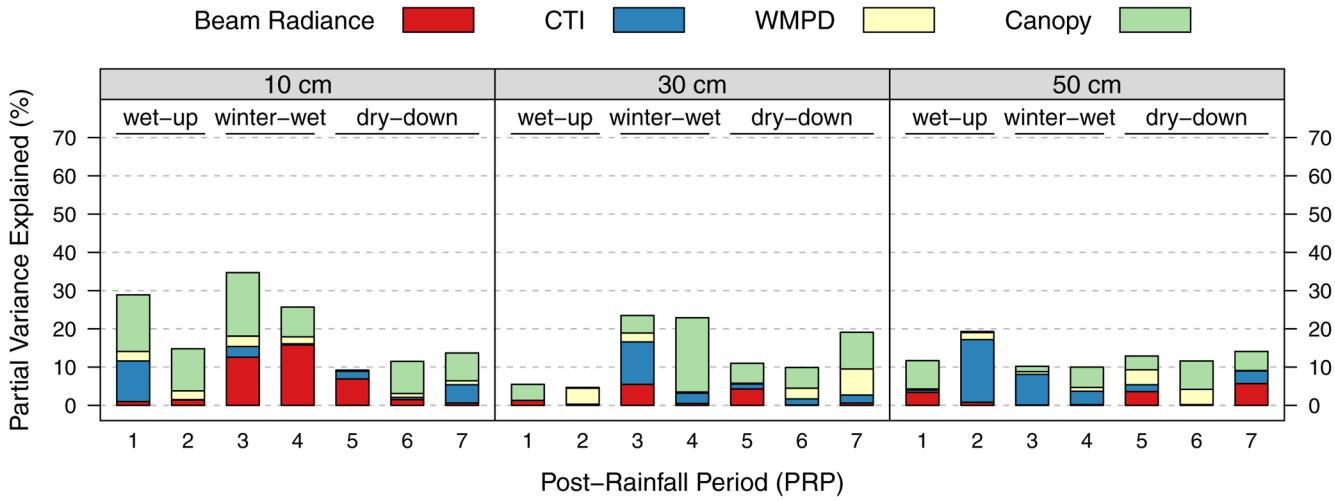

Fig. 10. Partial variance in the change in volumetric water content (ΔVWC) at Sierra Foothill Research and Extension Center (SFREC) explained by beam radiance, compound topographic index (CTI), weighted mean particle diameter (WMPD), and canopy cover, by post rainfall periods (PRPs) and sensor depth. Partial variances sum to approximately the total variance explained by multiple regression.

depth (Western et al., 1999; Swarowsky et al., 2012). Proxies for effective precipitation (CTI) and microclimate (annual beam radiance) accounted for a larger proportion of explained variance in ΔVWC, as compared with explained variance in $\overline{\text{VWC}}$, while the opposite was true for WMPD.

As for SJER, CTI was a dominant explanatory variable for predicting soil moisture content in a semiarid catchment in the Coast Ranges of California (Chamran et al., 2002). These Coast Range soils closely resemble those of SJER in terms of degree of argillic horizon expression (weakly developed or completely absent). The diminished capacity of CTI to explain variance in soil water content at SFREC may be due to the presence of a well-developed argillic horizon, and its high degree of spatial variability within the watershed. These findings suggest that stratifying studies relative to catena types (e.g., degree of soil development and/or soil stratigraphic characteristics) may improve our understanding of which DEM derived proxies work best across a range of soil properties and landscape attributes.

Further Investigation of Partial Effects at San Joaquin Experimental Range

Partial effects were investigated at SJER to determine the intensity of changes and temporal variation in $\overline{\text{VWC}}$ along gradients of CTI and modeled beam radiance. Partial effects were not examined at SFREC, due to the very small proportion of variance explained in VWC by either CTI or modeled beam radiance. Interpretation of a partial effect on $\overline{\text{VWC}}$ is based on the sign, magnitude, and standard error of the partial slope fit to a single predictor variable (e.g., CTI) within a multiple regression model, when all other predictor variables are held constant. Partial effects are presented in terms of a four unit change in CTI (roughly equivalent to moving from summit to backslope or backslope to swale position at SJER), and in terms of a 300 MJ/m^2 change in modeled beam radiance (roughly equivalent to moving from a north-facing to south-facing slope at SJER).

At 10 and 30 cm, the partial effect of CTI on $\overline{\text{VWC}}$ at SJER was always positive (i.e., higher $\overline{\text{VWC}}$ associated with larger values of CTI), significantly different than 0 in most PRPs, and generally increased in value over the course of the water year (Fig. 11). The partial effect of CTI on $\overline{\text{VWC}}$ was strongest at 30 and 50 cm, however, confidence in the estimate of this effect was best at 10 cm. The sign of the partial effect of CTI follows soil moisture patterns suggested by the standard hillslope model: lower positions in the landscape (larger CTI) are significantly wetter than higher positions in the landscape (smaller CTI). In addition, the magnitude of this relationship was greatest during the spring dry-down phase (PRP 5, 6, 7) when inputs from precipitation were less frequent and the redistribution of soil moisture reflects recharge and discharge areas across the catenas. This effect was probably masked during the winter wet phase (PRP 3 and 4) due to the greater homogeneity of soil moisture caused by frequent rainfall. Observations from SJER suggest that soils found on backslope positions will have approximately 2% (absolute) greater VWC compared to soils found on summit positions (i.e., a four unit increase in CTI) during the early winter wet-up phase, all else equal (Fig. 11). Similarly, a four unit change in CTI results in approximately 6 to 8% (absolute) greater VWC during the spring dry-down phase, all else equal. While these partial effect sizes seem small, they are significant with respect to the range in VWC within any given PRP. For example, at the 10-cm depth within PRP 1, the inter-quartile range of VWC was approximately 3 to 5% compared to approximately 5 to 7% during PRP 7.

The partial effect of modeled beam radiance on $\overline{\text{VWC}}$ at SJER was either negative or close to 0 at the 10-cm depth and not significantly different than 0 at 30- or 50-cm depths (Fig. 12). Temporal patterns in the magnitude and confidence in the partial effect of modeled beam radiance on $\overline{\text{VWC}}$ mirror temporal patterns in partial explained variance (Fig. 7), with the strongest and most precise estimates during the early winter wet-up phase (PRP 1 and 2) at 10 cm, and during the last PRP (at all depths) associated with the spring dry-down phase. Observations from SJER suggest that in similar landscapes and within post-rainfall dry-down events, a change of 300 MJ/m^2 of beam radiation (i.e., moving from a north- to south-facing slope) will result in approximately 1 to 3% (absolute) lower VWC at 10-cm depth (Fig. 12). While the magnitude of differences in soil moisture along gradients in modeled beam radiance (0–0.04 m^3/m^3 on north- vs. south-facing slopes at SJER) were slight, the cumulative effect is likely related to significant differentiation in soil-forming environments over time (Reid, 1973; Beaudette and O'Geen, 2009).

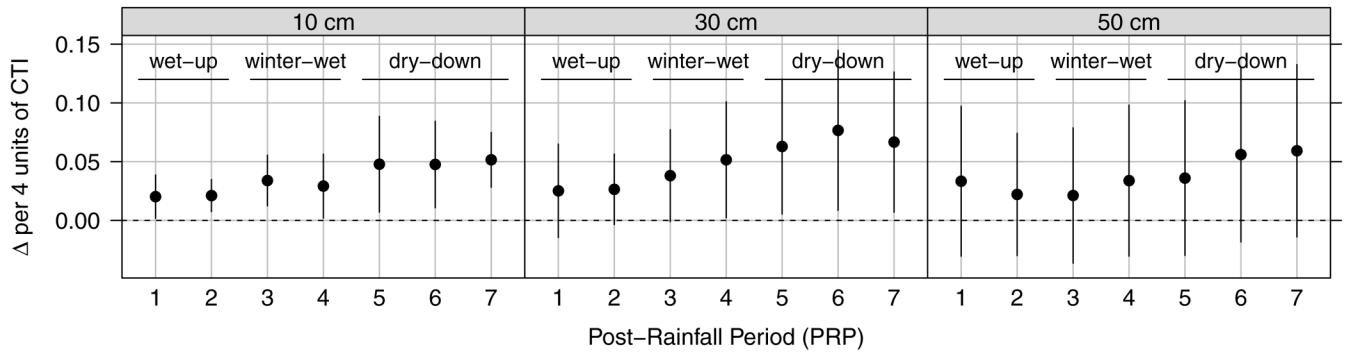

Fig. 11. Partial effect of compound topographic index (CTI) on meant volumetric water content ($\overline{\text{VWC}}$) at San Joaquin Experimental Range (SJER), with 95% confidence envelope (line segments). Units on the y axis represent the change in $\overline{\text{VWC}}$ expected for a four-unit increase in CTI, for each event. In landscapes similar to SJER, a four-unit increase in CTI represents moving from the summit to backslope position, or from backslope to swale position.

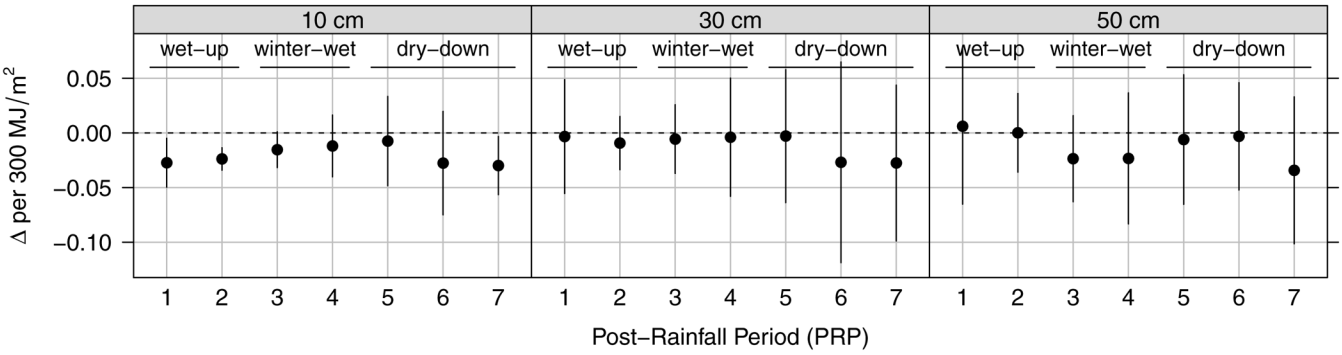

Fig. 12. Partial effect of summed beam radiance on the mean volumetric water content ($\overline{VWC}$) at San Joaquin Experimental Range (SJER), with 95% confidence envelope (line segments). Units on the y axis represent the change in $\overline{VWC}$ expected for a 300 MJ/m^2 increase in summed beam radiance, for each event. In landscapes similar to SJER, this change in beam radiance is roughly equal to moving from north-facing hillslope positions to south-facing hillslope positions.

CONCLUSIONS

After adjusting for differences due to water-holding capacity (using WMPD) and canopy cover, it was clear that spatial patterns in soil moisture and dry-down rates were more predictable in the more weakly developed granitic landscapes (SJER) as compared to the more highly developed metavolcanic landscapes (SFREC). No single terrain-shape index (GRAD, TCURV, PCURV, MCURV, PROM, TCI, and CTI) consistently accounted for the majority of variability in either $\overline{VWC}$ or ΔVWC, across depth or study site. However, at SJER, a combination of CTI and modeled beam radiance was able to consistently account for 30 to 70% of the total variance in $\overline{VWC}$ at 10 cm, and 10 to 40% at 30 and 50 cm. During the early winter wet-up and spring dry-down phases at SJER a combination of CTI and modeled beam radiance was able to consistently account for 30 to 60% of the total variance in ΔVWC at all depths. The degree to which soil moisture dynamics were explained by a combination of terrain and microclimate proxies was better than most studies (generally <50% explained variance) at SJER, and not surprisingly low at SFREC given the complex patchwork of soils with argillic horizons that form perched water tables. It is likely that variation in soil depth and contact type (paralithic vs. lithic) within both landscapes reduced the precision of our approach to partitioning explained variance in θ_v at depths of 50 cm.

Soil systems contain multiple, variably coupled, feedback mechanisms some of which simultaneously control (and are controlled by) soil moisture dynamics. Over geologic time scales, hillslope-scale differences in soil moisture affect pedogenic expression of soil properties and horizonation. In turn, differences in soil properties and horizonation alter the hydrologic behavior of the hillslope. Over seasonal and annual time scales, vegetation patterns adjust to favorable soil conditions; compounding the magnitude of spatial variability in soil moisture. In the less developed soils at SJER, soil stratigraphy and textural differences play less of a role in the redistribution of soil moisture resulting in spatial patterns that more closely match the scale of proxies used in this study. In the more highly developed soils at SFREC, the wide range in argillic horizon depth, thickness, and texture change, coupled with differences in vegetation density, likely had a strong impact on lateral and vertical redistribution of water; resulting in spatial patterns of soil moisture much smaller than the scale of our selected proxies. This study demonstrates that (within landscapes similar to the Sierra Foothill Region of California) the interpretation of DEM-derived proxies for soil moisture dynamics vary widely in time and space.

ACKNOWLEDGMENTS

We thank Alexandre Swarowsky and Tony Orozco for their efforts involved with excavation, soil description, and soil moisture sensor installation within the SFREC and SJER catenas. We would also like to thank Jaiyou Deng for his contributions to laboratory work supporting this study, and the staff at SJER and SFREC for their support. We thank Dr. Emilio Laca for his review of statistical methods and interpretations in this study. This work was funded by the Kearney Foundation of Soil Science.

REFERENCES

Beaudette, D.E., and A.T. O'Geen. 2009. Quantifying the aspect effect: An application of solar radiation modeling for soil survey. Soil Sci. Soc. Am. J. 73:1345–1352. doi:10.2136/sssaj2008.0229

Beven, K., and M. Kirkby. 1979. A physically based, variable contributing area model of basin hydrology. Bull. Int. Assoc. Sci. Hydrol. 24:43–69. doi:10.1080/02626667909491834

Bouman, C., and M. Shapiro. 1994. A multiscale random field model for bayesian image segmentation. IEEE Trans. Image Process. 3:162–177. doi:10.1109/83.277898

Burt, T., and D. Butcher. 1985. Topographic controls of soil moisture distributions. Eur. J. Soil Sci. 36:469–486. doi:10.1111/j.1365-2389.1985.tb00351.x

Campling, P., A. Gobin, and J. Feyen. 2002. Logistic modeling to spatially predict the probability of soil drainage classes. Soil Sci. Soc. Am. J. 66:1390–1401. doi:10.2136/sssaj2002.1390

Chamran, F., P.E. Gessler, and O.A. Chadwick. 2002. Spatially explicit treatment of soil-water dynamics along a semiarid catena. Soil Sci. Soc. Am. J. 66:1571–1583. doi:10.2136/sssaj2002.1571

Chow, A.T., S.T. Lee, A.T. O'Geen, T. Orozco, D. Beaudette, P.-K. Wong et al. 2009. Litter contributions to dissolved organic matter and disinfection byproduct precursors in California oak woodland watersheds. J. Environ. Qual. 38:2334–2343. doi:10.2134/jeq2008.0394

Dahlgren, R.A., M. Singer, and X. Huang. 1997. Oak tree and grazing impacts on soil properties and nutrients in a California oak woodland. Biogeochemistry 39:45–64. doi:10.1023/A:1005812621312

de Gruijter, J., D. Brus, M. Bierkens, and M. Knotters. 2006. Sampling for natural resource monitoring. Springer, New York.

Freer, J., J.J. McDonnell, K.J. Beven, N.E. Peters, D.A. Burns, R.P. Hooper et al. 2002. The role of bedrock topography on subsurface storm flow. Water Resour. Res. 38(12):1269. doi:10.1029/2001WR000872

Gordon, D., and K. Rice. 1992. Partitioning of space and water between

two California annual grassland species. Am. J. Bot. 79:967–976. doi:10.2307/2444905
GRASS Development Team. 2009. Geographic Resources Analysis Support System (GRASS GIS) Software. ITC-irst, Trento, Italy.
Grayson, R., and A. Western. 2001. Terrain and the distribution of soil moisture. Hydrol. Processes 15:2689–2690. doi:10.1002/hyp.479
Hacker, B.R. 1993. Evolution of the northern Sierra Nevada metamorphic belt: Petrological, structural, and Ar/Ar constraints. Geol. Soc. Am. Bull. 105:637–656. doi:10.1130/0016-7606(1993)105<0637:EOTNSN>2.3.CO;2
Harrell, F.E. 2001. Regression modeling strategies. Springer Series in Statistics. Springer, New York.
Holmes, T., and K. Rice. 1996. Patterns of growth and soil-water utilization in some exotic annuals and native perennial bunchgrasses of California. Ann. Bot. (Lond.) 78:233–243. doi:10.1006/anbo.1996.0117
Hudson, B.D. 1992. The soil survey as paradigm-based science. Soil Sci. Soc. Am. J. 56:836–841. doi:10.2136/sssaj1992.03615995005600030027x
Jackson, L., R. Strauss, M. Firestone, and J. Bartolome. 1990. Influence of tree canopies on grassland productivity and nitrogen dynamics in deciduous oak savanna. Agric. Ecosyst. Environ. 32:89–105. doi:10.1016/0167-8809(90)90126-X
Kasten, F. 1996. The Linke turbidity factor based on improved values of the integral Rayleigh optical thickness. Sol. Energy 56:239–244. doi:10.1016/0038-092X(95)00114-7
Legendre, P., and L. Legendre. 1998. Numerical ecology In: Developments in environmental modeling. 2nd ed. Number 20. Elsevier, Amsterdam, the Netherlands. http://www.sciencedirect.com/science/bookseries/01678892/20 (accessed 9 July 2013).
Lin, H., J. Bouma, Y. Pachepsky, A. Western, J. Thompson, R. van Genuchten et al. 2006. Hydropedology: Synergistic integration of pedology and hydrology. Water Resour. Res. 42:W05301. doi:10.1029/2005WR004085
Llobera, M. 2001. Building past landscape perception with GIS: Understanding topographic prominence. J. Archaeol. Sci. 28:1005–1014. doi:10.1006/jasc.2001.0720
McBratney, A.B., M.L. Mendonca Santos, and B. Minasny. 2003. On digital soil mapping. Geoderma 117:3–52. doi:10.1016/S0016-7061(03)00223-4
McGlynn, B.L., J.J. McDonnell, and D.D. Brammer. 2002. A review of the evolving perceptual model of hillslope flowpaths at the Maimai catchments, New Zealand. J. Hydrol. 257:1–26. doi:10.1016/S0022-1694(01)00559-5
McKenzie, N.J., P.E. Gessler, P.J. Ryan, and D.A. O'Connell. 2000. The role of terrain analysis in soil mapping. In: J.P. Wilson and J.C. Gallant, editors, Terrain analysis. John Wiley & Sons, New York. p. 245–265.
McKenzie, N.J., and P.J. Ryan. 1999. Spatial prediction of soil properties using environmental correlation. Geoderma 89:67–94. doi:10.1016/S0016-7061(98)00137-2
Mitasova, H., and J. Hofierka. 1993. Interpolation by regularized spline with tension: II. Application to terrain modeling and surface geometry analysis. Math. Geol. 25:657–669. doi:10.1007/BF00893172
Mitasova, H., and L. Mitas. 1993. Interpolation by regularized spline with tension: I. Theory and implementation. Math. Geol. 25:641–655. doi:10.1007/BF00893171
Moore, I., R. Grayson, and A. Ladson. 1991. Digital terrain modelling: A review of hydrological, geomorphological, and biological applications. Hydrol. Processes 5:3–30. doi:10.1002/hyp.3360050103
Moore, I.D., P.E. Gessler, G.A. Nielsen, and G.A. Peterson. 1993. Soil attribute prediction using terrain analysis. Soil Sci. Soc. Am. J. 57:443–452. doi:10.2136/sssaj1993.03615995005700020026x
Natural Resources Conservation Service. 1990. Soil survey. USDA, Madera Area, CA.
Natural Resources Conservation Service. 1998. Soil survey of Yuba County. USDA, Yuba County, CA.
Owe, M., E.B. Jones, and T.J. Schmugge. 1982. Soil moisture variation patterns observed in Hand County, South Dakota. Water Resour. Bull. 18:949–954. doi:10.1111/j.1752-1688.1982.tb00100.x
Pachepsky, Y.A., D.J. Timlin, and W.J. Rawls. 2001. Soil water retention as related to topographic variables. Soil Sci. Soc. Am. J. 65:1787–1795. doi:10.2136/sssaj2001.1787
Park, S., K. McSweeney, and B. Lowery. 2001. Identification of the spatial distribution of soils using a process-based terrain characterization. Geoderma 103:249–272. doi:10.1016/S0016-7061(01)00042-8
Park, S.J., and N. van de Giesen. 2004. Soil-landscape delineation to define spatial sampling domains for hillslope hydrology. J. Hydrol. 295:28–46. doi:10.1016/j.jhydrol.2004.02.022
Pennock, D.J., B.J. Zebarth, and E. De Jong. 1987. Landform classification and soil distribution in hummocky terrain, Saskatchewan, Canada. Geoderma 40:297–315. doi:10.1016/0016-7061(87)90040-1
Rains, M. C., G.E. Fogg, T. Harter, R.A. Dahlgren, and R.J. Williamson. 2006. The role of perched aquifers in hydrological connectivity and biogeochemical processes in vernal pool landscapes, Central Valley, California. Hydrol. Processes 20:1157–1175. doi:10.1002/hyp.5937
Redding, T.E., and K.J. Devito. 2008. Lateral flow thresholds for aspen forested hillslopes on the Western Boreal Plain, Alberta, Canada. Hydrol. Processes 22:4287–4300. doi:10.1002/hyp.7038
Reid, I. 1973. The influence of slope orientation upon the soil moisture regime, and its hydrogeomorphological significance. J. Hydrol. 19:309–321. doi:10.1016/0022-1694(73)90105-4
Reynolds, S.G. 1970. The gravimetric method of soil moisture determination, Part III: An examination of factors influencing soil moisture variability. J. Hydrol. 11:288–300. doi:10.1016/0022-1694(70)90068-5
Rigollier, C., O. Bauer, and L. Wald. 2000. On the clear sky model of the ESRA–European Solar Radiation Atlas–with respect to the Heliosat method. Sol. Energy 68:33–48. doi:10.1016/S0038-092X(99)00055-9
Scull, P., J. Franklin, O. Chadwick, and D. McArthur. 2003. Predictive soil mapping: A review. Prog. Phys. Geogr. 27:171–197. doi:10.1191/0309133303pp366ra
Soil Survey Staff. 2004. Soil survey laboratory methods manual. 4th ed. Number 42 In: Soil survey investigations report. USDA-NRCS, Washington, DC.
Strand, R. 1967. Geologic map of California: Mariposa sheet. Technical report. California Division of Mines and Geology. ftp://ftp.consrv.ca.gov/pub/dmg/pubs/gam/GAM_009_Mariposa/GAM_009_Explanation_1967.pdf (accessed 9 July 2013).
Swarowsky, A., R.A. Dahlgren, K.W. Tate, J.W. Hopmans, and A.T. O'Geen. 2011. Catchment-scale soil water dynamics in a Mediterranean-type oak woodland. Vadose Zone J. 10:800–815. doi:10.2136/vzj2010.0126
Swarowsky, A., R.A. Dahlgren, and A.T. O'Geen. 2012. Linking subsurface lateral flowpath activity with streamflow characteristics in a semiarid headwater catchment. Soil Sci. Soc. Am. J. 76:532–547. doi:10.2136/sssaj2011.0061
Takagi, K., and H.S. Lin. 2011. Temporal dynamics of soil moisture spatial variability in the Shale Hills critical zone observatory. Vadose Zone J. 10:832–842. doi:10.2136/vzj2010.0134
Thompson, J.A., J.C. Bell, and C.A. Butler. 2001. Digital elevation model resolution: Effects on terrain attribute calculation and quantitative soil-landscape modeling. Geoderma 100:67–89. doi:10.1016/S0016-7061(00)00081-1
Tromp-van Meerveld, H.J., and J.J. McDonnell. 2006. Threshold relations in subsurface stormflow 2. The fill and spill hypothesis. Water Resour. Res. 42:1–8.
Tromp-van Meerveld, H.J., N.E. Peters, and J.J. McDonnell. 2007. Effect of bedrock permeability on subsurface stormflow and the water balance of a trenched hillslope at the Panola Mountain Research Watershed, Georgia, USA. Hydrol. Processes 21:750–769. doi:10.1002/hyp.6265
Verzani, J. 2004. Using R for Introductory Statistics. Chapman & Hal, Norwell, MA.
Wagenet, R.J., J. Bouma, and J.L. Hutson. 1994. Modeling water and chemical fluxes as driving forces of pedogenesis. In: R.B. Bryant and R.W. Arnold, editors, Quantitative modeling of soil forming processes. SSSA Spec. Publ. 39. SSSA, Madison, WI. p. 17–36.
Western, A.W., and G. Blöschl. 1999. On the spatial scaling of soil moisture. J. Hydrol. 217:203–224. doi:10.1016/S0022-1694(98)00232-7
Western, A.W., R.B. Grayson, G. Blöschl, G.R. Willgoose, and T.A. McMahon. 1999. Observed spatial organization of soil moisture and its relation to terrain indices. Water Resour. Res. 35:797–810. doi:10.1029/1998WR900065
Wilding, L.P., J. Bouma, and D.W. Goss. 1994. Impact of spatial variability on interpretive modeling. p. 61–70. In: R.B. Bryant and R.W. Arnold, editors, Quantitative modeling of soil forming processes. SSSA Spec. Publ. 39. SSSA, Madison, WI.
Wilson, J.P., and J.C. Gallant. 2000a. Digital terrain analysis. In: J.P. Wilson and J.C. Gallant, editors, Terrain analysis: Principles and applications. John Wiley & Sons, New York. p. 1–27.
Wilson, J.P., and J.C. Gallant. 2000b. Secondary terrain attributes. In: J.P. Wilson and J.C. Gallant, editors, Terrain analysis: Principles and applications. John Wiley & Sons, New York. p. 87–131.